Squeezing Limit of the Josephson Ring Modulator as a Nondegenerate Parametric Amplifier

Dong Hwan Kim,* Su-Yong Lee,† Zaeill Kim, Taek Jeong, and Duk Y. Kim
Agency for Defense Development, Daejeon 34186, Korea

(Received 22 June 2022; revised 17 January 2023; accepted 1 February 2023; published 6 March 2023)

Two-mode squeezed vacuum states are a crucial component of quantum technologies. In the microwave domain, they can be produced by the Josephson ring modulator that acts as a three-wave mixing nondegenerate parametric amplifier. Here, we numerically solve the full master equation of three bosonic modes describing the Josephson ring modulator to compute squeezing of output fields and gain at low signal power. We show that the third-order interaction from the three-wave mixing process intrinsically limits squeezing and reduces gain. Since our results are related to other general cavity-based three-wave mixing processes, these imply that any nondegenerate parametric amplifier will have an intrinsic squeezing limit in the output fields.

DOI: 10.1103/PhysRevApplied.19.034015

I. INTRODUCTION

Two-mode squeezed vacuum (TMSV) states are widely used in quantum technologies, such as continuous-variable quantum teleportation [1,2], quantum metrology [3,4], quantum dense coding [5], and quantum illumination [6–8]. TMSV states, which consist of signal and idler modes, are usually generated via nondegenerate three-wave or four-wave mixing processes with the help of a strong pump beam [2,9–12]. Systems with such interactions are called nondegenerate parametric amplifiers (NDPAs). For applications in long distance target detection, preparation of TMSV states in the microwave range is beneficial. In microwave quantum technology, Josephson junctions provide nonlinearity for generation of squeezed states [13,14].

Ideal parametric amplifiers are systems with quadratic Hamiltonians, which are approximated via physical nonlinearities and external pumps. However, high-order terms of the Josephson junction potential have a negative effect on squeezing and gain in the degenerate parametric amplifier [15,16]. For generation of TMSV states, we consider the NDPA, where the signal, idler, and pump modes each interact with different modes of a cavity. The Josephson ring modulator (JRM) structure acts as a NDPA, having advantages in that signal and idler modes are well separated in space and frequency [17,18]. The effect of high-order terms of the JRM on saturation power was studied in Ref. [19] using a semiclassical approach. To identify the effect of the actual JRM Hamiltonian on squeezing, we perform a quantum analysis of the NDPA master equation with three interacting bosonic modes in the frequency domain, which is a computationally intensive task due to the massive size of the density matrix. Previously, stochastic methods were studied to bypass this problem in the time domain under other systems [20,21], whereas obtaining frequency domain information from these methods is not straightforward. We instead develop a numerical method to solve the master equation on commercial computers and compute squeezing of the JRM output field along with gain at low signal power. We observe a limit in squeezing and find the fundamental reason by examining several different Hamiltonians.

II. JRM HAMILTONIAN AND APPROXIMATIONS

The JRM consists of four identical Josephson junctions in a ring connected to external capacitors to form a microwave cavity as shown in Fig. 1(a). The Josephson energy $E_J = \hbar\omega_J$ and Josephson inductance L_J are related via $E_J = \phi_0^2/L_J$, where $\phi_0 = \hbar/2e$ is the flux quantum. By adding additional internal inductors L_{in}, it is possible to operate the JRM at the Kerr nulling point, where all even-order interactions are zero [19]. The ratio of inductances $\beta = L_J/L_{\text{in}}$ controls the overall strength of nonlinearity. As the energy scales of inductors are inversely proportional to inductance, high β implies small nonlinearity of the JRM.

The JRM has three resonance modes, $\hat{a}$, $\hat{b}$, and $\hat{c}$, which we refer to as the signal, idler, and pump modes, respectively. The Hamiltonian of the JRM with an external pump

*kiow639@add.re.kr
†suyong2@add.re.kr

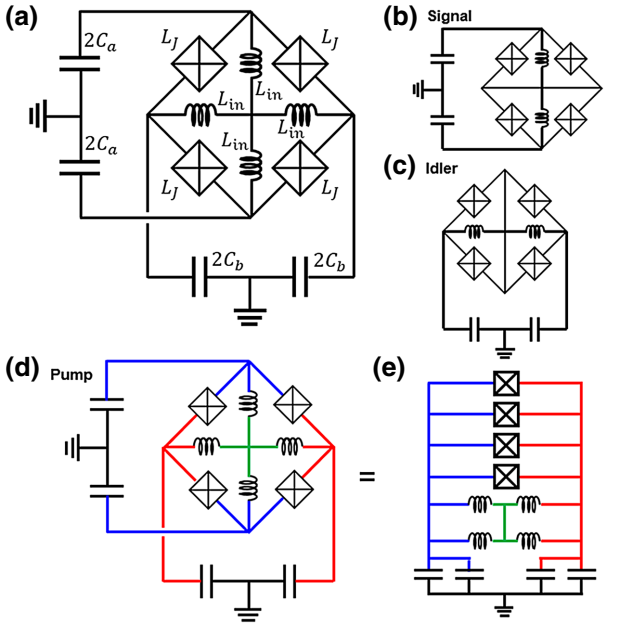

FIG. 1. (a) Circuit structure of the JRM. Four identical Josephson junctions form a ring, connected to external capacitors. Internal inductors are added to operate at the Kerr nulling point. (b),(c),(d) *LC* circuit structure of the three resonance modes: signal, idler, pump, respectively. (e) Equivalent circuit of (d), to clarify the *LC* circuit structure.

on mode $\hat{c}$ is

$$H_{\rm JRM} = \sum_{m=a,b,c} \omega_m \hat{m}^\dagger \hat{m} + i\epsilon(\hat{c}^\dagger e^{-i\omega_P t} - \hat{c} e^{i\omega_P t}) - 4\omega_J \sin\frac{\hat{\varphi}_a}{2} \sin\frac{\hat{\varphi}_b}{2} \sin\hat{\varphi}_c, \quad (1)$$

where ω_a, ω_b, and ω_c are resonance frequencies of the cavity. The external pump frequency is $\omega_P \simeq \omega_a + \omega_b$, and ϵ describes the external pump on mode $\hat{c}$. The resonance frequencies are determined by the (linearized) *LC* circuits in Figs. 1(b), 1(c), 1(e). The mode fluxes $\hat{\varphi}_m$ are related to quadrature operators $\hat{x}_m = (1/\sqrt{2})(\hat{m} + \hat{m}^\dagger)$, $m = a, b, c$, as

$$\hat{\varphi}_a = \sqrt{\frac{2\omega_a}{\beta\omega_J}}\hat{x}_a, \qquad \hat{\varphi}_b = \sqrt{\frac{2\omega_b}{\beta\omega_J}}\hat{x}_b, \qquad \hat{\varphi}_c = \sqrt{\frac{\omega_c}{\beta\omega_J}}\hat{x}_c. \quad (2)$$

Details of the quantization procedure are given in Appendix A.

The linear approximation of $\sin\hat{\varphi} \simeq \hat{\varphi}$ with the rotating-wave approximation (RWA) gives the third-order three-wave mixing Hamiltonian. In a frame rotating at input field frequencies ω_S, ω_I, and ω_P for modes $\hat{a}$, $\hat{b}$, and $\hat{c}$, respectively, the approximation of Eq. (1) is

$$H_3 = \sum_{m=a,b,c} \Delta_m \hat{m}^\dagger \hat{m} + i\epsilon\hat{c}^\dagger + i\sqrt{\frac{\omega_a\omega_b\omega_c}{2\beta^3\omega_J}}\hat{a}\hat{b}\hat{c}^\dagger + \text{c. c.}, \quad (3)$$

where $\Delta_a = \omega_a - \omega_S$, $\Delta_b = \omega_b - \omega_I$, and $\Delta_c = \omega_c - \omega_P$ are detunings between cavity resonances and input fields. The phase of each mode is adjusted for the prefactor i of interaction. The fifth-order approximation H_5 is obtained by adding terms from $\hat{\varphi}_a^3\hat{\varphi}_b\hat{\varphi}_c$, $\hat{\varphi}_a\hat{\varphi}_b^3\hat{\varphi}_c$, and $\hat{\varphi}_a\hat{\varphi}_b\hat{\varphi}_c^3$ in the sine power series to H_3. The stiff pump approximation Hamiltonians H_{3s} and H_{5s}, where back action of signal and idler modes on the pump is neglected, arise from replacing $\hat{c}$ with $\epsilon/(\kappa_c/2 + i\Delta_c)$ in H_3 and H_5. [22]. The third-order stiff pump approximation Hamiltonian is the NDPA model Hamiltonian:

$$H_{3s} = H_{\rm NDPA} = \sum_{m=a,b} \Delta_m \hat{m}^\dagger \hat{m} + i(g\hat{a}\hat{b} - g^*\hat{a}^\dagger\hat{b}^\dagger), \quad (4)$$

$$g = \sqrt{\frac{\omega_a\omega_b\omega_c}{2\beta^3\omega_J}}\frac{\epsilon}{(\kappa_c/2 - i\Delta_c)}. \quad (5)$$

For the system of Eq. (4), squeezing and gain both increase unboundedly as pump power increases below a threshold power. Above this threshold, the system becomes unstable.

The whole JRM Hamiltonian is described by matrix elements of $\sin\alpha\hat{x}$ that are a sum of matrix elements of displacement operators [23]. In general, $\langle n|\sin\alpha\hat{x}|m\rangle$ is nonzero when n and m have different parities. For small α, the matrix elements $\langle n|\sin\alpha\hat{x}|n \pm 1\rangle$ are dominant among all matrix elements; hence, we approximate the sine potential with only transitions like $\hat{a}\hat{b}\hat{c}^\dagger$ or $\hat{a}^\dagger\hat{b}^\dagger\hat{c}$, denoted as H_{J1}. Applying the RWA, the next contribution comes from transitions like $\hat{a}^3\hat{b}^3\hat{c}^{\dagger 3}$, which have smaller matrix elements than $\hat{a}\hat{b}\hat{c}^\dagger$-like transitions. We verified that considering these transitions does not affect the results obtained from H_{J1}. Explicit formulas for the Hamiltonians are given in Appendix A.

III. NUMERICAL METHODS

Squeezing S is computed from output field moments as

$$S = 10\,\text{Log}_{10}\frac{2}{\Delta}, \quad (6)$$

where

$$\Delta = \text{Var}(\hat{X}_-) + \text{Var}(\hat{P}_+), \quad (7)$$

$$\hat{X}_- = \frac{1}{\sqrt{2}}(\hat{a}_{\rm out} + \hat{a}_{\rm out}^\dagger - e^{i\phi}\hat{b}_{\rm out} - e^{-i\phi}\hat{b}_{\rm out}^\dagger), \quad (8)$$

$$\hat{P}_+ = \frac{1}{i\sqrt{2}}(\hat{a}_{\rm out} - \hat{a}_{\rm out}^\dagger + e^{i\phi}\hat{b}_{\rm out} - e^{-i\phi}\hat{b}_{\rm out}^\dagger), \quad (9)$$

$\hat{a}_{\rm out}$ and $\hat{b}_{\rm out}$ are output operators of the signal and idler modes, respectively, and ϕ is defined to minimize Δ. It is known that $\Delta \geq 2$ for separable states [24,25]. For a three-wave mixing process, the minimum of Δ is

$$\frac{\Delta_{\rm min}}{2} = \langle \hat{a}^\dagger_{\rm out}\hat{a}_{\rm out}\rangle + \langle \hat{b}^\dagger_{\rm out}\hat{b}_{\rm out}\rangle + 1 - 2|\langle \hat{a}_{\rm out}\hat{b}_{\rm out}\rangle|. \quad (10)$$

It is possible to compute output field moments from the master equation and input-output relations, as shown in Appendix B and Ref. [26]:

$$\dot{\rho} = -i[H,\rho] + \sum_{m=a,b,c}\frac{\kappa_m}{2}\mathcal{D}_{\hat{m}}[\rho] =: \mathcal{L}[\rho], \quad (11)$$

$$\hat{m}_{\rm out} = \sqrt{\kappa_m}\hat{m} - \hat{m}_{\rm in}, \qquad m = a,b,c, \quad (12)$$

with $\hat{m}_{\rm in(out)}$ input (output) operators of each mode. Here $\mathcal{D}_{\hat{m}}[\rho] := 2\hat{m}\rho\hat{m}^\dagger - \rho\hat{m}^\dagger\hat{m} - \hat{m}^\dagger\hat{m}\rho$ gives dissipation and κ_m is the mode decay rate. For calculating the moments in the frequency domain, the steady state $\rho_{\rm ss}$ of the master equation and expressions like $\mathcal{L}^{-1}[\hat{a}\rho_{\rm ss}]$ are needed. Both quantities are obtained by solving the master equations $\mathcal{L}[\rho_{\rm ss}] = 0$ and $\mathcal{L}[\tilde{\rho}] = \hat{a}\rho_{\rm ss}$. This is a nontrivial task, because there are $O(n^4n_c^2)$ variables describing the density matrix when considering n levels for the signal and idler modes each and n_c levels for the pump mode. However, the master equations of three-wave mixing processes are block diagonal, where blocks are defined by $a_1 - b_1 - a_2 + b_2 = (\text{const.})$, $\rho = \sum \rho^{a_2b_2c_2}_{a_1b_1c_1}|a_1,b_1,c_1\rangle\langle a_2,b_2,c_2|$, so we only need to solve on each block. We denote the subspace with $a_1 - b_1 - a_2 + b_2 = k$ as V_k. The steady state is concentrated on V_0, and the number of variables in V_0 is $O(n^3n_c^2)$. After reducing variables, the problem requires a reasonable amount of memory allowing us to solve the problem.

We numerically solve the master equation using the BiCGSTAB algorithm [27] implemented in MATLAB®. The stopping criterion is 10^{-10} error in relative residual. Initial guesses and preconditioning, which are additional inputs for the algorithm, are important for convergence and computational efficiency. Initial guesses come from the NDPA model with the stiff pump approximation. We can exactly solve the master equation of the NDPA model, so solutions from the NDPA model serve as initial guesses for the master equations of other systems, as shown in Appendix C.

Preconditioning is, loosely speaking, forming an approximate inverse of the problem. For preconditioning, we solve the master equation related to the Hamiltonian

$$H = \Delta_a\hat{a}^\dagger\hat{a} + \Delta_b\hat{b}^\dagger\hat{b} + \Delta_c\hat{c}^\dagger\hat{c} + i\epsilon(\hat{c}^\dagger - \hat{c}). \quad (13)$$

Equation (11) with the above Hamiltonian is solvable at a cheap cost, as the equation is block upper diagonal, where blocks are defined by constants a_1, b_1, a_2, and b_2. We use a one-step red-black Gauss-Seidel iteration as the preconditioner for better performance [28]. Red-black partitioning is done via the parity of $a_1 - a_2$. Reducing variables, analytically solving the NDPA model, and identifying an appropriate block structure for preconditioning are the main contributions for making the master equation a tractable problem.

TABLE I. Truncation levels n and n_c used with respect to expected gain G_0. The first n, n_c levels are used in the computation.

	G_0 (dB)				
	1–14	15–17	18	19	20
n	20	30	34	36	40
n_c ($\beta = 3,5,7$)	20	20	20	20	20
n_c ($\beta = 10$)	30	30	30	30	30

It is also possible to compute gain at low signal power. Phase-preserving gain is defined as

$$G = 10\,\text{Log}_{10}\left|\frac{\langle\hat{a}_{\rm out}\rangle}{\langle\hat{a}_{\rm in}\rangle}\right|^2. \quad (14)$$

If the input field of the signal mode is a coherent state with parameter α, this effectively adds $i\sqrt{\kappa_a}(\alpha\hat{a}^\dagger - \alpha^*\hat{a})$ to the Hamiltonian. Using a perturbative approach, we write the steady state as $\rho_{\rm ss}(\alpha) = \rho_{\rm ss} + \alpha\rho_1 + \alpha^*\rho_1^\dagger + \cdots$. The steady-state equation at order α is $\mathcal{L}[\rho_1] + \sqrt{\kappa_a}[\hat{a}^\dagger, \rho_{\rm ss}] = 0$. Here $\rho_{\rm ss}$ is the steady state with vacuum input that has elements only in V_0, so $[\hat{a}^\dagger, \rho_{\rm ss}]$ has elements only in V_1. The same methods for computing initial guesses and preconditioning are applicable to finding ρ_1. Gain is obtained from

$$\frac{\langle\hat{a}_{\rm out}\rangle}{\langle\hat{a}_{\rm in}\rangle} = \left.\frac{\partial\langle\hat{a}_{\rm out}\rangle}{\partial\alpha}\right|_{\alpha=0} = \sqrt{\kappa_a}\,\text{Tr}(\hat{a}\rho_1) - 1, \quad (15)$$

using the boundary condition (12). When setting pump power ϵ to achieve expected gain G_0 in the NDPA model, the actual gain G will differ from G_0. We define this difference as *reduction in gain*, $(G - G_0)/G_0$.

Here, we set the system parameters as $\omega_a = 7.5 \times 2\pi$ GHz, $\omega_b = 5 \times 2\pi$ GHz, $\kappa_a = \kappa_b = \kappa_c = 100 \times 2\pi$ MHz, $i_c = 1\ \mu$A as in Ref. [19], $\Delta_a = \Delta_b = 0$, and $\omega_P = \omega_a + \omega_b$. The truncation level n of the signal and idler modes and the truncation level n_c of the pump mode are set as in Table I. We determine n so that the error in S from truncation is less than 1 % in the NDPA model. The required pump power for the same gain increases as β^3 [see Eq. (3)], so considering higher levels of the pump mode is necessary when solving problems with high β. The obtained numerical values converge as n and n_c increase. For problems with the stiff pump approximation, we set $n = 40$ and directly solve the master equation.

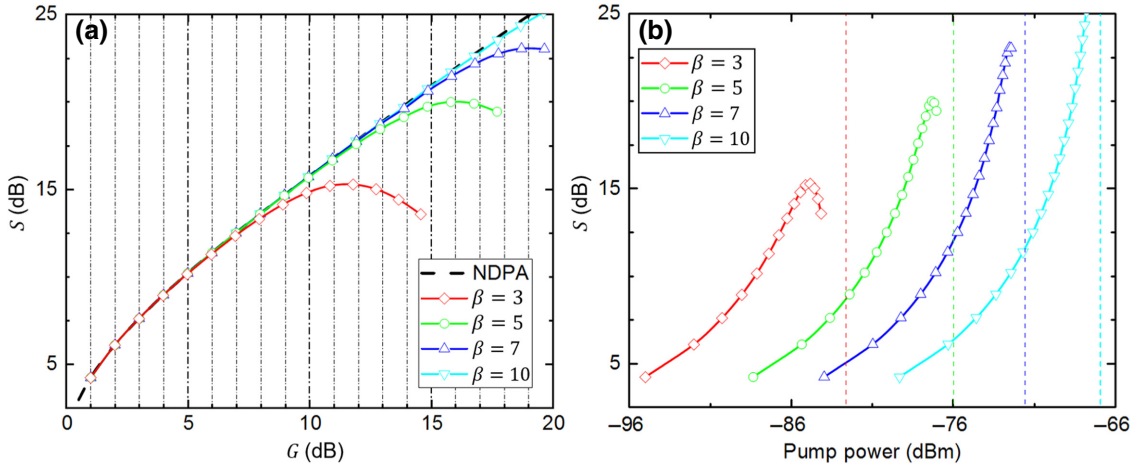

FIG. 2. Squeezing S as a function of (a) actual gain G or (b) pump power under Hamiltonian H_{J1}. We compare four systems $\beta = 3, 5, 7, 10$ with the ideal NDPA model. Points indicated with markers are actual results for integer values of expected gain G_0. The left shift of markers compared to the vertical dashed lines in (a) shows the difference between actual gain G and expected gain G_0. Vertical dashed lines in (b) represent the threshold power of each system.

IV. RESULTS

Figure 2(a) shows S as a function of actual gain G for $\beta = 3, 5, 7, 10$, using Hamiltonian H_{J1}. There is a maximal point for S in terms of G, which limits the operation of the JRM as an entanglement source. For each β, squeezing of the JRM is similar to that of the ideal NDPA model at low gain, while it starts to deviate from the NDPA model with increasing gain. Systems with higher β (smaller nonlinearity) start to deviate from the NDPA model at higher gain. We plot the same results with respect to the pump power in Fig. 2(b). To achieve the same squeezing or gain, a higher pump power is required for systems with smaller nonlinearity. However, this would heat up the system, adding thermal fluctuations or other spurious effects that also limit squeezing. This implies that there will be an optimal β for the JRM as a squeezing source in realistic systems.

To understand the mechanism of the squeezing limit, we compute S and G with respect to various Hamiltonians, $H_{3s} = H_{\mathrm{NDPA}}$, H_{5s}, H_3, H_5, and H_{J1}. Figure 3 shows S and $(G - G_0)/G_0$ respectively computed from the Hamiltonians with $\beta = 3$. The squeezing limit appears for the full third-order Hamiltonian H_3, whereas squeezing from H_{5s} does not deviate from the NDPA model. This shows that the three-wave mixing term $\hat{a}\hat{b}\hat{c}^\dagger$ itself imposes a bound on squeezing. Such an effect is not profound in the optical regime using nonlinear crystals, where the main limiting factor is attributed to optical losses [29]. However, a decrease in squeezing at high pump power was observed experimentally with the JRM in Ref. [8]. Squeezing is

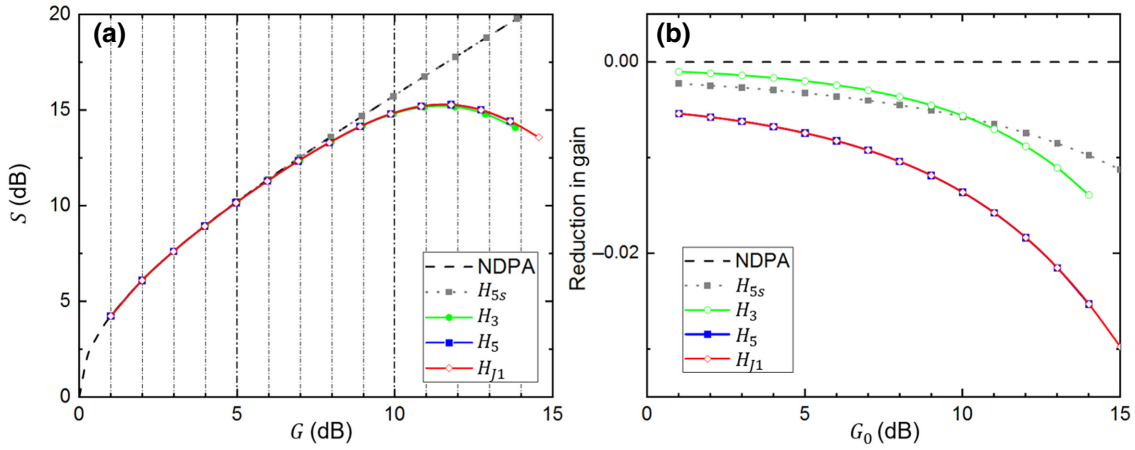

FIG. 3. (a) Squeezing S as a function of actual gain G under various Hamiltonians with $\beta = 3$. The Hamiltonians are $H_{3s} = H_{\mathrm{NDPA}}$, H_{5s}, H_3, H_5, and H_{J1}. (b) Reduction in gain $(G - G_0)/G_0$ as a function of expected gain G_0 under the various Hamiltonians in (a). Results for H_5 overlap with those for H_{J1}. The red lines of H_{J1} here correspond to the red lines in Fig. 2.

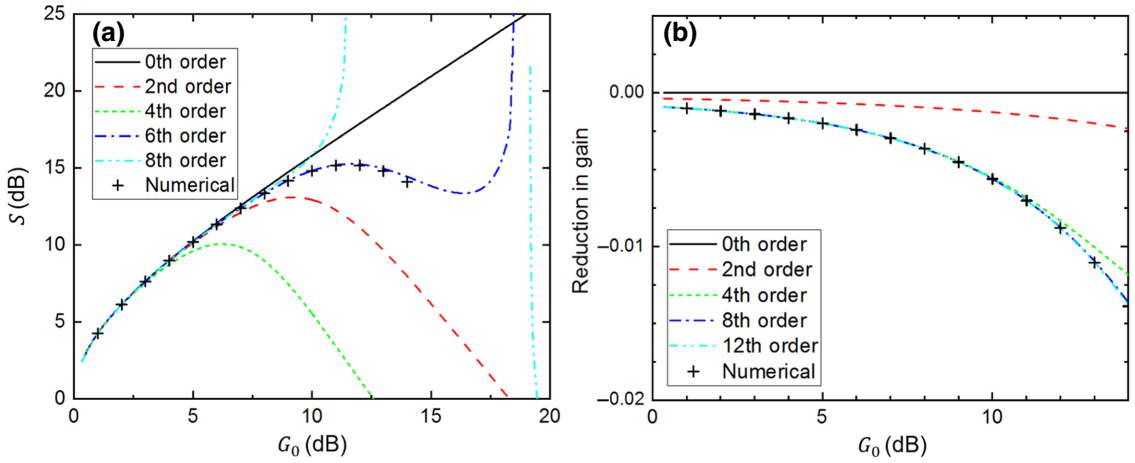

FIG. 4. (a) Squeezing S and (b) reduction in gain $(G - G_0)/G_0$ as a function of expected gain G_0 for the Padé approximants and numerical results under $\beta = 3$ and H_3. Zeroth-order results and numerical results here correspond to the results of NDPA and H_3 in Fig. 3, respectively.

a delicate process, in which various losses, broadened bandwidth of realistic detectors, system instability, and so on can restrict its performance. Excluding these extrinsic factors, our results show that the three-wave mixing interaction $\hat{a}\hat{b}\hat{c}^\dagger$ itself intrinsically limits squeezing, providing fundamental insight into this interaction.

Figure 3(b) shows $(G - G_0)/G_0$ under various Hamiltonians. The decrease in gain from fifth-order terms, H_{5s}, is easily understood as the fifth-order terms effectively reducing the three-wave mixing coupling constant depending on the mean photon number of each mode. Even for the H_3 Hamiltonian, there is a reduction in gain that is comparable to the drop introduced from the fifth-order terms, H_{5s}. Again, the $\hat{a}\hat{b}\hat{c}^\dagger$ term itself reduces gain.

To further verify that the $\hat{a}\hat{b}\hat{c}^\dagger$ term is responsible for altering S and G, we use a power-series expansion in solving the third-order Hamiltonian H_3. Displacing mode $\hat{c}$ by $-\epsilon/(\kappa_c/2 + i\Delta_c)$, the master equation becomes $\dot{\rho} = \mathcal{L}_0[\rho] + \mathcal{L}_1[\rho]$ with

$$\mathcal{L}_0[\rho] = -i[H_0, \rho] + \sum_{m=a,b,c} \frac{\kappa_m}{2} \mathcal{D}_{\hat{m}}[\rho], \tag{16}$$

$$\mathcal{L}_1[\rho] = \sqrt{\frac{\omega_a \omega_b \omega_c}{2\beta^3 \omega_J}} [\hat{a}\hat{b}\hat{c}^\dagger - \hat{a}^\dagger \hat{b}^\dagger \hat{c}, \rho], \tag{17}$$

where $H_0 = H_{\mathrm{NDPA}} + \Delta_c \hat{c}^\dagger \hat{c}$. Treating $\mathcal{L}_1$ as a perturbation, the zeroth-order steady state ρ_0 is nothing but a two-mode squeezed thermal state in modes $\hat{a}$, $\hat{b}$ and vacuum in mode $\hat{c}$. The actual steady state is $\rho_{\mathrm{ss}} = (I + \mathcal{L}_0^{-1}\mathcal{L}_1)^{-1}[\rho_0]$, so we can write ρ_{ss} as a power series in $\mathcal{L}_1$, provided it converges. The output field moments and gain are computable through ρ_{ss} and $\mathcal{L}^{-1} = (\mathcal{L}_0 + \mathcal{L}_1)^{-1}$, so we can write these in a power series of $\mathcal{L}_1$. The power series is then converted to Padé approximants for better accuracy [30]. Figure 4 shows S and $(G - G_0)/G_0$ of various approximants and the numerical results under $\beta = 3$ and H_3. As S is the logarithm of a small positive value, it is much more prone to approximation errors. The difference in moments can be negative in some cases, giving the divergences for sixth- and eighth-order plots in Fig. 4(a). Meanwhile Fig. 4(b) shows that the approximants appropriately account for the reduction in gain. All nonzero terms in the perturbation series start with either $\hat{a}\hat{b}\hat{c}^\dagger\rho_0$ or $\rho_0\hat{a}^\dagger\hat{b}^\dagger\hat{c}$. This implies that the signal and idler loss channels from $\hat{a}\hat{b}\hat{c}^\dagger$ are the main reason for the declines in S and G.

V. CONCLUSION

We numerically solve the master equation of the JRM and compute squeezing of the output fields. Numerical analysis of such large-scale problems requires specifically tailored algorithms. We develop an algorithm based on solving the master equation only consisting of free terms, loss terms, and pump interactions. This means that our algorithm is applicable to systems utilizing strong pumps, which is typical in nonlinear systems. For example, the master equation of degenerate parametric amplification can also be fully solved by our algorithm, which is directly related to single-mode squeezed state generation in both microwave and optical frequencies. Furthermore, our algorithm is parallelizable for high-performance computers, as shown in Appendix D; hence, it can enable quantum mechanical treatments of nonlinear systems that were not possible before.

We show the existence of a fundamental limit in two-mode squeezing from nondegenerate parametric amplification. The three-wave mixing term $\hat{a}\hat{b}\hat{c}^\dagger$ itself bounds squeezing S and also reduces gain as it introduces another

loss channel to the signal and idler modes. A power-series expansion is also computed to support the results. For any general NDPA using three-wave mixing, the leading-order interaction is given as that of Eq. (3) regardless of the actual physical system. Thus, our results describe the physics of general three-wave mixing NDPA.

Results of the full sine potential of the JRM are close to those of the fifth-order Hamiltonian. Increasing β decreases the overall nonlinearity of the JRM, and the maximum achievable S increases. However, as nonlinearity decreases, a stronger pump is required for the same squeezing or gain, and then other effects such as heating from the pump can also limit S. A recent study about Josephson traveling-wave parametric amplifiers also observed a reduction in squeezing at high gain [12]. We suggest that the strong nonlinear interaction itself could cause the squeezing limit in other Josephson-junction-based systems. Our study can be utilized in designing microwave devices for quantum enhanced sensing and measurements.

ACKNOWLEDGMENTS

This work is supported by a grant to the Defense-Specialized Project funded by the Defense Acquisition Program Administration and Agency for Defense Development.

APPENDIX A: QUANTUM HAMILTONIAN OF THE JRM

The classical Hamiltonian of the Josephson ring modulator at the Kerr nulling point is given as [19]

$$H = \frac{1}{4\phi_0^2}\left(\frac{2q_a^2}{C_a} + \frac{2q_b^2}{C_b} + \frac{(C_a+C_b)q_c^2}{2C_aC_b}\right) + \frac{\phi_0^2}{4L_{\text{in}}}(\varphi_a^2+\varphi_b^2+2\varphi_c^2) - \frac{4\phi_0^2}{L_J}\sin\frac{\varphi_a}{2}\sin\frac{\varphi_b}{2}\sin\varphi_c. \tag{A1}$$

The resonance frequencies are

$$\omega_a^2 = \frac{1}{2C_aL_{\text{in}}}, \qquad \omega_b^2 = \frac{1}{2C_bL_{\text{in}}}, \qquad \omega_c^2 = \frac{C_a+C_b}{4C_aC_bL_{\text{in}}}. \tag{A2}$$

There is a relation $\omega_c^2 = \frac{1}{2}(\omega_a^2+\omega_b^2)$. Quantization is done by imposing

$$\hat{\varphi}_a = \sqrt{\frac{2\omega_a}{\beta\omega_J}}\hat{x}_a, \qquad \hat{\varphi}_b = \sqrt{\frac{2\omega_b}{\beta\omega_J}}\hat{x}_b, \qquad \hat{\varphi}_c = \sqrt{\frac{\omega_c}{\beta\omega_J}}\hat{x}_c, \tag{A3}$$

$$\hat{q}_a = \hbar\sqrt{\frac{\beta\omega_J}{2\omega_a}}\hat{p}_a, \qquad \hat{q}_b = \hbar\sqrt{\frac{\beta\omega_J}{2\omega_b}}\hat{p}_b, \quad \hat{q}_c = \hbar\sqrt{\frac{\beta\omega_J}{\omega_c}}\hat{p}_c, \tag{A4}$$

where $\hat{x}_m = (1/\sqrt{2})(\hat{m}^\dagger+\hat{m})$, $\hat{p}_m = (i/\sqrt{2})(\hat{m}^\dagger-\hat{m})$ $(m=a,b,c)$. Then the Hamiltonian is

$$H_{\text{JRM}} = \sum_{m=a,b,c}\hbar\omega_m\hat{m}^\dagger\hat{m} - 4\hbar\omega_J\sin\frac{\hat{\varphi}_a}{2}\sin\frac{\hat{\varphi}_b}{2}\sin\hat{\varphi}_c. \tag{A5}$$

We add a pump term to H_{JRM} and move to a rotating frame at input field frequencies ω_S, ω_I, ω_P. Applying the RWA and linearizing the sine potential gives the third-order Hamiltonian

$$H_3 = \sum_{m=a,b,c}\Delta_m\hat{m}^\dagger\hat{m} + i\epsilon(\hat{c}^\dagger-\hat{c}) + i\sqrt{\frac{\omega_a\omega_b\omega_c}{2\beta^3\omega_J}}(\hat{a}\hat{b}\hat{c}^\dagger-\hat{a}^\dagger\hat{b}^\dagger\hat{c}). \tag{A6}$$

Adding the next-order contribution of the sine potential gives the fifth-order Hamiltonian

$$H_5 = H_3 - i\sqrt{\frac{\omega_a\omega_b\omega_c}{8\beta^5\omega_J^3}}\left[\frac{\omega_a}{2}(\hat{a}^\dagger\hat{a}+1)\hat{a}\hat{b}\hat{c}^\dagger + \frac{\omega_b}{2}(\hat{b}^\dagger\hat{b}+1)\hat{a}\hat{b}\hat{c}^\dagger + \omega_c\hat{a}\hat{b}\hat{c}^\dagger(\hat{c}^\dagger\hat{c}+1)\right] + \text{c.c.} \tag{A7}$$

Replacing $\hat{c}$ with $\epsilon/(\kappa_c/2+i\Delta_c)$ in H_3, H_5 leads to the stiff-pump approximation Hamiltonians

$$H_{3s} = H_{\text{NDPA}} = \sum_{m=a,b}\Delta_m\hat{m}^\dagger\hat{m} + i(g\hat{a}\hat{b} - g^*\hat{a}^\dagger\hat{b}^\dagger), \qquad g = \sqrt{\frac{\omega_a\omega_b\omega_c}{2\beta^3\omega_J}}\frac{\epsilon}{(\kappa_c/2-i\Delta_c)}, \tag{A8}$$

$$H_{5s} = H_{3s} - \frac{g}{2\beta\omega_J}\left[\frac{\omega_a}{2}(\hat{a}^\dagger\hat{a}+1)\hat{a}\hat{b} + \frac{\omega_b}{2}(\hat{b}^\dagger\hat{b}+1)\hat{a}\hat{b} + \omega_c\hat{a}\hat{b}\left(\frac{\epsilon^2}{\kappa_c^2/4+\Delta_c^2}+1\right)\right] + \text{c.c.} \tag{A9}$$

The explicit form of matrix elements of $\sin\alpha\hat{x}$ is obtained from writing $\sin\alpha\hat{x}$ as a sum of two displacement operators

[23]. For n and m with different parities,

$$\langle n|\sin\alpha\hat{x}|m\rangle = e^{-\alpha^2/4}\sqrt{\frac{\min(n,m)!}{\max(n,m)!}}\frac{\alpha}{\sqrt{2}} \times\left(-\frac{\alpha^2}{2}\right)^{(|n-m|-1)/2} L^{|n-m|}_{\min(n,m)}\left(\frac{\alpha^2}{2}\right), \tag{A10}$$

where the L^a_n are the generalized Laguerre polynomials. The constant term of L^a_n is $\binom{n+a}{n}$, so, for small fixed α, the matrix elements $|\langle n|\sin\alpha\hat{x}|n+k\rangle|$ decay in k as

$$|\langle n|\sin\alpha\hat{x}|n+k\rangle| \propto \sqrt{\frac{n!}{(n+k)!}}\left(\frac{\alpha}{\sqrt{2}}\right)^k\binom{n+k}{n} \propto \sqrt{\frac{(n+k)!}{k!^2}}\left(\frac{\alpha}{\sqrt{2}}\right)^k. \tag{A11}$$

Retaining only $\hat{a}\hat{b}\hat{c}^\dagger$-like interactions of the JRM sine potential, we obtain the Hamiltonian

$$H_{J1} = \sum_{m=a,b,c}\Delta_m\hat{m}^\dagger\hat{m} + i\epsilon(\hat{c}^\dagger - \hat{c}) + i\sqrt{\frac{\omega_a\omega_b\omega_c}{2\beta^3\omega_J}}e^{-(\omega_a+\omega_b+2\omega_c)/8\beta\omega_J} \times\sum_{n_a,n_b,n_c} L^1_{n_a}\left(\frac{\omega_a}{4\beta\omega_J}\right)L^1_{n_b}\left(\frac{\omega_b}{4\beta\omega_J}\right)L^1_{n_c}\left(\frac{\omega_c}{2\beta\omega_J}\right) \times\frac{|n_a,n_b,n_c+1\rangle\langle n_a+1,n_b+1,n_c|}{\sqrt{(n_a+1)(n_b+1)(n_c+1)}} + \text{c.c.} \tag{A12}$$

APPENDIX B: SOLVING THE NDPA VIA INPUT-OUTPUT THEORY

The ideal NDPA Hamiltonian in a frame rotating at the signal and idler frequencies (ω_s, ω_i, respectively) is

$$H_{\text{NDPA}} = \Delta_a\hat{a}^\dagger\hat{a} + \Delta_b\hat{b}^\dagger\hat{b} + ig(e^{-i\theta}\hat{a}\hat{b} - e^{i\theta}\hat{a}^\dagger\hat{b}^\dagger), \tag{B1}$$

where $\Delta_a := \omega_a - \omega_s$ and $\Delta_b := \omega_b - \omega_i$ are detunings of cavity resonances from signal and idler frequencies, and $g > 0$ is the coupling strength. Defining the Fourier transform as

$$f[\omega] = \int\frac{dt}{\sqrt{2\pi}}f(t)e^{i\omega t}, \tag{B2}$$

we can write the equation of motion of operators and input-output relations in the frequency domain as

$$\begin{bmatrix}\sqrt{\kappa_a} & \\ & \sqrt{\kappa_b}\end{bmatrix}\begin{bmatrix}\hat{a}_i[\omega]\\ \hat{b}_i[-\omega]^\dagger\end{bmatrix} = \begin{bmatrix}i(\Delta_a-\omega)+\kappa_a/2 & ge^{i\theta}\\ ge^{-i\theta} & -i(\Delta_b+\omega)+\kappa_b/2\end{bmatrix}\begin{bmatrix}\hat{a}[\omega]\\ \hat{b}[-\omega]^\dagger\end{bmatrix}, \tag{B3}$$

$$\begin{bmatrix}\hat{a}_o[\omega]\\ \hat{b}_o[-\omega]^\dagger\end{bmatrix} = \begin{bmatrix}\sqrt{\kappa_a} & \\ & \sqrt{\kappa_b}\end{bmatrix}\begin{bmatrix}\hat{a}[\omega]\\ \hat{b}[-\omega]^\dagger\end{bmatrix} - \begin{bmatrix}\hat{a}_i[\omega]\\ \hat{b}_i[-\omega]^\dagger\end{bmatrix}. \tag{B4}$$

Here κ_a and κ_b are the mode decay rates that describe dissipation. Solving the equations gives

$$\begin{bmatrix}\hat{a}_o[\omega]\\ \hat{b}_o[-\omega]^\dagger\end{bmatrix} = \left(\begin{bmatrix}\sqrt{\kappa_a} & \\ & \sqrt{\kappa_b}\end{bmatrix}\begin{bmatrix}i(\Delta_a-\omega)+\kappa_a/2 & ge^{i\theta}\\ ge^{-i\theta} & -i(\Delta_b+\omega)+\kappa_b/2\end{bmatrix}^{-1}\begin{bmatrix}\sqrt{\kappa_a} & \\ & \sqrt{\kappa_b}\end{bmatrix} - 1\right)\begin{bmatrix}\hat{a}_i[\omega]\\ \hat{b}_i[-\omega]^\dagger\end{bmatrix} = S[\omega]\begin{bmatrix}\hat{a}_i[\omega]\\ \hat{b}_i[-\omega]^\dagger\end{bmatrix}. \tag{B5}$$

Defining susceptibilities as

$$\chi_a^{-1} := \frac{\kappa_a}{2} + i(\Delta_a - \omega), \qquad \chi_b^{-1} := \frac{\kappa_b}{2} + i(\Delta_b + \omega), \tag{B6}$$

we can write

$$S_{11} = \frac{g^2 + (\chi_a^*)^{-1}(\chi_b^*)^{-1}}{\chi_a^{-1}(\chi_b^*)^{-1} - g^2}, \qquad S_{12} = \frac{-g\sqrt{\kappa_a\kappa_b}e^{i\theta}}{\chi_a^{-1}(\chi_b^*)^{-1} - g^2}, \tag{B7}$$

$$S_{21} = \frac{-g\sqrt{\kappa_a\kappa_b}e^{-i\theta}}{\chi_a^{-1}(\chi_b^*)^{-1} - g^2}, \qquad S_{22} = \frac{g^2 + \chi_a^{-1}\chi_b^{-1}}{\chi_a^{-1}(\chi_b^*)^{-1} - g^2}. \tag{B8}$$

The low power gain is $|S_{11}|^2$. The nonzero second-order moments are

$$\langle\hat{a}_o[\omega]^\dagger\hat{a}_o[\omega]\rangle = |S_{12}|^2, \qquad \langle\hat{b}_o[-\omega]^\dagger\hat{b}_o[-\omega]\rangle = |S_{21}|^2, \qquad \langle\hat{a}_o[\omega]\hat{b}_o[-\omega]\rangle = S_{11}S_{21}^*. \tag{B9}$$

We have omitted a factor of $\delta(0)$ that comes from $[\hat{a}_o[\omega_1], \hat{a}_o[\omega_2]^\dagger] = \delta(\omega_1 - \omega_2)$. We also have omitted a factor of $\delta(0)$ in the numerical results of the main text, which corresponds to considering an ideal detector of a very narrow bandwidth.

APPENDIX C: SOLVING THE NDPA VIA THE QUANTUM REGRESSION THEOREM

We solve the ideal NDPA by the methods described in the main text. The calculations are more complicated than the above scattering matrix approach in the frequency domain. The purpose of doing these calculations is twofold: verify that this approach is equivalent to the scattering matrix approach and provide appropriate initial guesses for the numerical methods used in solving the full Hamiltonian. The master equation describing the dynamics of the density operator is

$$\dot{\rho} = -i[H_{\mathrm{NDPA}}, \rho] + \frac{\kappa_a}{2}\mathcal{D}_{\hat{a}}[\rho] + \frac{\kappa_b}{2}\mathcal{D}_{\hat{b}}[\rho] =: \mathcal{L}[\rho], \tag{C1}$$

where $\mathcal{D}_{\hat{a}}[\rho] := 2\hat{a}\rho\hat{a}^\dagger - \rho\hat{a}^\dagger\hat{a} - \hat{a}^\dagger\hat{a}\rho$ gives dissipation and κ_a, κ_b are the mode decay rates.

1. Steady state and eigenmodes of the NDPA master equation

Inverting $\mathcal{L}$ amounts to finding all eigenmodes and eigenvalues of $\mathcal{L}$, where the eigenmode with eigenvalue 0 is the steady state and other eigenmodes are exponentially damped in time. It is possible to write eigenmodes in terms of characteristic functions, defined as

$$\chi_\rho(\alpha, \beta) = \mathrm{Tr}(\hat{D}(\alpha, \beta)\rho), \tag{C2}$$

where $\hat{D}(\alpha, \beta) = e^{\alpha\hat{a}^\dagger + \beta\hat{b}^\dagger - \mathrm{c.c.}}$ is the standard displacement operator. The master equation (C1) can be formulated for the characteristic function as

$$\begin{aligned}\dot{\chi} = &-i\Delta_a[-\alpha\partial_\alpha + \alpha^*\partial_{\alpha^*}]\chi - i\Delta_b[-\beta\partial_\beta + \beta^*\partial_{\beta^*}]\chi \\ &+ ge^{-i\theta}[\beta\partial_{\alpha^*} + \alpha\partial_{\beta^*}]\chi + ge^{i\theta}[\beta^*\partial_\alpha + \alpha^*\partial_\beta]\chi \\ &+ \frac{\kappa_a}{2}[-\alpha^*\partial_{\alpha^*} - \alpha\partial_\alpha - |\alpha|^2]\chi \\ &+ \frac{\kappa_b}{2}[-\beta^*\partial_{\beta^*} - \beta\partial_\beta - |\beta|^2]\chi.\end{aligned} \tag{C3}$$

One can show that the steady-state solution to the above equation is a Gaussian function:

$$\chi_{\mathrm{ss}}(\alpha, \beta) = e^{-q^\dagger\sigma q/2}, \qquad \sigma = \begin{bmatrix} s_1 & & & s_2 \\ & s_1 & s_3 & \\ & s_2 & s_4 & \\ s_3 & & & s_4 \end{bmatrix}. \tag{C4}$$

The coordinates q are $q = (\alpha, -\alpha^*, \beta, -\beta^*)^t$. This state is a two-mode squeezed thermal state. Entries of σ give the symmetrized moments of the steady state:

$$\begin{aligned} &s_1 = \langle\hat{a}^\dagger\hat{a}\rangle + \tfrac{1}{2}, \qquad s_2 = \langle\hat{a}\hat{b}\rangle, \qquad s_3 = \langle\hat{a}^\dagger\hat{b}^\dagger\rangle, \\ &s_4 = \langle\hat{b}^\dagger\hat{b}\rangle + \tfrac{1}{2}. \end{aligned} \tag{C5}$$

Specific values of s_1, s_2, s_3, s_4 are

$$s_1 = \frac{\kappa_a\kappa_b(\kappa^2 + 4\Delta^2) + 4g^2(-\kappa_a^2 + \kappa_b^2)}{2(\kappa^2(\kappa_a\kappa_b - 4g^2) + 4\kappa_a\kappa_b\Delta^2)}, \tag{C6}$$

$$s_2 = \frac{-2\kappa_a\kappa_b(\kappa - 2i\Delta)ge^{i\theta}}{\kappa^2(\kappa_a\kappa_b - 4g^2) + 4\kappa_a\kappa_b\Delta^2}, \tag{C7}$$

$$s_3 = \frac{-2\kappa_a\kappa_b(\kappa + 2i\Delta)ge^{-i\theta}}{\kappa^2(\kappa_a\kappa_b - 4g^2) + 4\kappa_a\kappa_b\Delta^2}, \tag{C8}$$

$$s_4 = \frac{\kappa_a\kappa_b(\kappa^2 + 4\Delta^2) + 4g^2(\kappa_a^2 - \kappa_b^2)}{2(\kappa^2(\kappa_a\kappa_b - 4g^2) + 4\kappa_a\kappa_b\Delta^2)}. \tag{C9}$$

We introduced the total loss $\kappa := \kappa_a + \kappa_b$ and total detuning $\Delta := \Delta_a + \Delta_b$. The number state expansion of this state contains terms only of the form

$$|n + \ell, n\rangle\langle m + \ell, m|, \qquad |n, n + \ell\rangle\langle m, m + \ell|. \tag{C10}$$

The coefficient of $|n + \ell, n\rangle\langle m + \ell, m|$ is

$$\begin{aligned}&4\frac{\kappa_a\kappa_b(\kappa^2 + 4\Delta^2) - 4\kappa^2g^2}{4\kappa_a\kappa_b(\kappa^2 + 4\Delta^2 - 4g^2)}\sqrt{\frac{(n + \ell)!\,(m + \ell)!}{n!\,m!\,\ell!^2}}a^\ell c^n d^m \\ &\quad\times {}_2F_1\left(-n, -m; \ell + 1; \frac{4g^2}{\kappa^2 + 4\Delta^2}\right)\end{aligned} \tag{C11}$$

and the coefficient of $|n, n + \ell\rangle\langle m, m + \ell|$ is

$$\begin{aligned}&4\frac{\kappa_a\kappa_b(\kappa^2 + 4\Delta^2) - 4\kappa^2g^2}{4\kappa_a\kappa_b(\kappa^2 + 4\Delta^2 - 4g^2)}\sqrt{\frac{(n + \ell)!\,(m + \ell)!}{n!\,m!\,\ell!^2}}b^\ell c^n d^m \\ &\quad\times {}_2F_1\left(-n, -m; \ell + 1; \frac{4g^2}{\kappa^2 + 4\Delta^2}\right),\end{aligned} \tag{C12}$$

where ${}_2F_1$ is the hypergeometric function and a, b, c, d are the numbers

$$\begin{aligned} a &= \frac{4\kappa_b g^2/\kappa_a}{\kappa^2 + 4\Delta^2 - 4g^2}, \qquad b = \frac{4\kappa_a g^2/\kappa_b}{\kappa^2 + 4\Delta^2 - 4g^2}, \\ c &= \frac{-2(\kappa + 2i\Delta)ge^{-i\theta}}{\kappa^2 + 4\Delta^2 - 4g^2}, \qquad d = \frac{-2(\kappa - 2i\Delta)ge^{i\theta}}{\kappa^2 + 4\Delta^2 - 4g^2}. \end{aligned} \tag{C13}$$

The other eigenmodes of (C3) can be found from the steady state. For some function f, the eigenvalue problem of

$\chi = f\,\chi_{\rm ss}$ can be written in terms of f as

$$\begin{aligned}\lambda f \;=& -i\Delta_a[-\alpha\partial_\alpha + \alpha^*\partial_{\alpha^*}]f \; - i\Delta_b[-\beta\partial_\beta + \beta^*\partial_{\beta^*}]f \\ &+ ge^{-i\theta}[\beta\partial_{\alpha^*} + \alpha\partial_{\beta^*}]f \; + ge^{i\theta}[\beta^*\partial_\alpha + \alpha^*\partial_\beta]f \\ &+ \frac{\kappa_a}{2}[-\alpha^*\partial_{\alpha^*} - \alpha\partial_\alpha]f \; + \frac{\kappa_b}{2}[-\beta^*\partial_{\beta^*} - \beta\partial_\beta]f\,.\end{aligned} \tag{C14}$$

If f is a homogeneous polynomial in $\alpha, \alpha^*, \beta, \beta^*$ then the right-hand side of Eq. (C14) is a homogeneous polynomial of the same degree; hence, the eigenfunctions f will be homogeneous polynomials. Also, the variable α is coupled only with β^*, so f will be a product of two polynomials, one with variables α, β^* and the other with variables α^*, β. This reflects the fact that the NDPA mixes the operator $\hat{a}$ only with $\hat{b}^\dagger$.

The degree-1 solutions of Eq. (C14) are the building blocks of general eigenmodes. The solutions in variables α, β^* have eigenvalues

$$\lambda_\pm = \tfrac{1}{2}\big[-(\chi_a^*)^{-1} - \chi_b^{-1} \pm \sqrt{(-(\chi_a^*)^{-1} + \chi_b^{-1})^2 + 4g^2}\big] \tag{C15}$$

with $\chi_m^{-1} = \kappa_m/2 + i\Delta_m$ $(m = a, b)$. The corresponding eigenfunctions are

$$f_+ = \xi\alpha + 2ge^{i\theta}\beta^*, \qquad f_- = \xi\beta^* - 2ge^{-i\theta}\alpha, \tag{C16}$$

$$\xi = -(\chi_a^*)^{-1} + \chi_b^{-1} + \sqrt{(-(\chi_a^*)^{-1} + \chi_b^{-1})^2 + 4g^2}. \tag{C17}$$

The degree-1 eigenvalues, eigenfunctions of variables α^*, β are simply given by complex conjugates, $\lambda_+^*, \lambda_-^*, f_+^*, f_-^*$. General eigenmodes of Eq. (C14) are products of these functions:

$$f_{nm\ell k} = f_+^n f_+^{*m} f_-^{*\ell} f_-^k, \quad \lambda_{nm\ell k} = n\lambda_+ + m\lambda_+^* + \ell\lambda_-^* + k\lambda_-. \tag{C18}$$

Then characteristic functions of the eigenmodes of the master equation are $\chi_{nm\ell k} = f_{nm\ell k}\chi_{\rm ss}$. Finally, we note that multiplication by α, α^* on χ corresponds to $[\rho, \hat{a}]$, $[\rho, \hat{a}^\dagger]$, respectively, so, with Eqs. (C11) and (C12), it is possible to compute the number basis representations of these states. In the following, we refrain from explicitly working with eigenmodes and instead use the fact that $\mathcal{L}$ preserves the degree of f when acting on a state with characteristic function $\chi = f\,\chi_{\rm ss}$.

2. Output field moments of the NDPA

We compute $\langle \hat{a}_o[\omega]\hat{b}_o[-\omega]\rangle$ using the quantum regression theorem. The integral over $dt_1 dt_2$ is split over time orderings and $\tau = |t_1 - t_2|$:

$$\begin{aligned}\langle \hat{a}_o[\omega_1]\hat{b}_o[\omega_2]\rangle &= \frac{1}{2\pi}\int dt_1 dt_2 \;\langle \hat{a}_o(t_1)\hat{b}_o(t_2)\rangle\, e^{i\omega_1 t_1 + i\omega_2 t_2} \\ &= \frac{1}{2\pi}\left(\int_{t_1>t_2} + \int_{t_1<t_2}\right){\rm Tr}[\hat{a}_o(t_1)\hat{a}_o(t_2)\rho_{\rm ss}]e^{i\omega_1 t_1 + i\omega_2 t_2} \\ &= \delta(\omega_1+\omega_2)\int_0^\infty d\tau\;\; {\rm Tr}[\hat{a}_o(\tau)\hat{b}_o\rho_{\rm ss}]e^{i\omega_1\tau} + {\rm Tr}[\hat{b}_o(\tau)\hat{a}_o\rho_{\rm ss}]e^{i\omega_2\tau} \\ &= \delta(\omega_1+\omega_2)\sqrt{\kappa_a\kappa_b}\int_0^\infty d\tau\;\; {\rm Tr}[\hat{a}e^{\mathcal{L}\tau}[\hat{b}\rho_{\rm ss}]]e^{i\omega_1\tau} + {\rm Tr}[\hat{b}e^{\mathcal{L}\tau}[\hat{a}\rho_{\rm ss}]]e^{i\omega_2\tau} \\ &= \delta(\omega_1+\omega_2)\sqrt{\kappa_a\kappa_b}\left({\rm Tr}\left[\hat{a}\frac{-1}{\mathcal{L}+i\omega_1}[\hat{b}\rho_{\rm ss}]\right] + {\rm Tr}\left[\hat{b}\frac{-1}{\mathcal{L}+i\omega_2}[\hat{a}\rho_{\rm ss}]\right]\right).\end{aligned} \tag{C19}$$

We have used the input-output relation $\hat{a}_o = \sqrt{\kappa_a}\hat{a}$ in Eq. (C19), which is valid under trace when the input field is vacuum. The characteristic function of $\hat{a}\rho_{\rm ss}$ is

$$\left(-\partial_{\alpha^*} - \frac{\alpha}{2}\right)\chi_{\rm ss} = [\alpha\chi_{\rm ss} \;\; \beta^*\chi_{\rm ss}]\begin{bmatrix} s_1 - \frac{1}{2} \\ -s_2\end{bmatrix}. \tag{C20}$$

Then the characteristic function of $-(\mathcal{L}+i\omega_2)^{-1}[\hat{a}\rho_{\rm ss}]$ is

$$[\alpha\chi_{\rm ss} \;\; \beta^*\chi_{\rm ss}]\left(-\begin{bmatrix} i\Delta_a - \kappa_a/2 & ge^{-i\theta} \\ ge^{i\theta} & -i\Delta_b - \kappa_b/2\end{bmatrix} - i\omega_2\right)^{-1} \begin{bmatrix} s_1 - \frac{1}{2} \\ -s_2\end{bmatrix}. \tag{C21}$$

This serves as an initial guess for the numerical computations of the full Hamiltonian. The trace of $-\hat{b}(\mathcal{L}+i\omega_2)^{-1}[\hat{a}\rho_{\rm ss}]$ is the negative of the coefficient of β^* in Eq. (C21). Hence we have

$$\mathrm{Tr}\left[\hat{b}\frac{-1}{\mathcal{L}+i\omega_2}[\hat{a}\rho_{\rm ss}]\right] = [0 \quad 1]\left(\begin{bmatrix} i\Delta_a-\kappa_a/2 & ge^{-i\theta} \\ ge^{i\theta} & -i\Delta_b-\kappa_b/2\end{bmatrix}+i\omega_2\right)^{-1}\begin{bmatrix} s_1-\frac{1}{2} \\ -s_2\end{bmatrix}. \tag{C22}$$

Similarly, we can compute

$$\mathrm{Tr}\left[\hat{a}\frac{-1}{\mathcal{L}+i\omega_1}[\hat{b}\rho_{\rm ss}]\right] = [1 \quad 0]\left(\begin{bmatrix} -i\Delta_a-\kappa_a/2 & ge^{-i\theta} \\ ge^{i\theta} & i\Delta_b-\kappa_b/2\end{bmatrix}+i\omega_1\right)^{-1}\begin{bmatrix} -s_2 \\ s_4-\frac{1}{2}\end{bmatrix}. \tag{C23}$$

Combining these results yields the same expression as Eq. (B9). Other moments are computed in the same way.

3. Gain at low signal power of the NDPA

As written in the main text, the gain at low signal power is computed from

$$\frac{\langle\hat{a}_o\rangle}{\langle\hat{a}_i\rangle} = \sqrt{\kappa_a}\mathrm{Tr}[\hat{a}\rho_1]-1, \qquad G = 10\,\mathrm{Log}_{10}\left|\frac{\langle\hat{a}_o\rangle}{\langle\hat{a}_i\rangle}\right|^2, \tag{C24}$$

where ρ_1 is the solution to $\mathcal{L}[\rho_1]=\sqrt{\kappa_a}[\rho_{\rm ss},\hat{a}^\dagger]$. The characteristic function of $[\rho_{\rm ss},\hat{a}^\dagger]$ is just $\alpha^*\chi_{\rm ss}$, so the characteristic function of ρ_1 is given as

$$\sqrt{\kappa_a}[\alpha^*\chi_{\rm ss}\ \beta\chi_{\rm ss}]\begin{bmatrix} -i\Delta_a-\kappa_a/2 & ge^{-i\theta} \\ ge^{i\theta} & i\Delta_b-\kappa_b/2\end{bmatrix}^{-1}\begin{bmatrix}1\\0\end{bmatrix}. \tag{C25}$$

Then we obtain the result of Eq. (B5):

$$\begin{aligned}\frac{\langle\hat{a}_o\rangle}{\langle\hat{a}_i\rangle} &= \kappa_a[1 \quad 0]\begin{bmatrix} i\Delta_a+\kappa_a/2 & -ge^{-i\theta} \\ -ge^{i\theta} & -i\Delta_b+\kappa_b/2\end{bmatrix}^{-1}\begin{bmatrix}1\\0\end{bmatrix}-1 \\ &= S_{11}[0].\end{aligned} \tag{C26}$$

APPENDIX D: PARALLELIZABILITY OF OUR ALGORITHM

Parallel computing is one of the key aspects in high-performance computing. We show how to parallelize our proposed preconditioner, which implies that our preconditioner can be implemented on high-performance computers. There is a block diagonal structure to the preconditioner allowing parallel computing. Recall that the preconditioner is based on solving the master equation given as

$$\mathcal{L}[\rho] := -i[H,\rho]+\sum_{m=a,b,c}\frac{\kappa_m}{2}\mathcal{D}_{\hat{m}}[\rho]=\sigma, \tag{D1}$$

$$H := \Delta_a\hat{a}^\dagger\hat{a}+\Delta_b\hat{b}^\dagger\hat{b}+\Delta_c\hat{c}^\dagger\hat{c}+i\epsilon(\hat{c}^\dagger-\hat{c}), \tag{D2}$$

$$\mathcal{D}_{\hat{m}}[\rho] := 2\hat{m}\rho\hat{m}^\dagger-\rho\hat{m}^\dagger\hat{m}-\hat{m}^\dagger\hat{m}\rho, \tag{D3}$$

where σ is an arbitrary vector obtained during the BiCGSTAB algorithm. We label the entries of ρ as coefficients of $|a_1,b_1,c_1\rangle\langle a_2,b_2,c_2|$. We first consider the block structure defined by constants a_1,a_2,b_1,b_2, so each block has n_c^2 variables, where n_c is the truncation level of the pump mode $\hat{c}$. The only terms in the master equation that couple different a_1,a_2,b_1,b_2 are the loss terms $\hat{a}\rho\hat{a}^\dagger$, $\hat{b}\rho\hat{b}^\dagger$. These terms always lower the value of a_1,a_2,b_1,b_2, so starting from the block with highest a_1,a_2,b_1,b_2, we can easily solve the master equation.

The loss terms $\hat{a}\rho\hat{a}^\dagger$, $\hat{b}\rho\hat{b}^\dagger$ preserve the values a_1-a_2, b_1-b_2, so there is a larger block structure where the master equation is block diagonal. In the larger block structure defined by constants a_1-a_2, b_1-b_2, the master equation is block diagonal and each block is block upper diagonal from the previous paragraph. This block diagonal structure allows us to parallelize our preconditioner. We further use a red-black Gauss-Seidel iteration where the red-black partitioning is based on the parity of a_1-a_2. This is compatible with the block structure defined by constants a_1-a_2, b_1-b_2, so our proposed preconditioner is parallelizable.

[1] S. L. Braunstein and H. J. Kimble, Teleportation of Continuous Quantum Variables, Phys. Rev. Lett. **80**, 869 (1998).
[2] A. Furusawa, J. L. Sørensen, S. L. Braunstein, C. A. Fuchs, H. J. Kimble, and E. S. Polzik, Unconditional quantum teleportation, Science **282**, 5389 (1998).
[3] P. M. Anisimov, G. M. Raterman, A. Chiruvelli, W. N. Plick, S. D. Huver, H. Lee, and J. P. Dowling, Quantum Metrology with Two-Mode Squeezed Vacuum: Partiy

Detection Beats the Heisenberg Limit, Phys. Rev. Lett. **104**, 103602 (2010).
[4] S. Steinlechner, J. Bauchrowitz, M. Meinders, H. Müller-Ebhardt, K. Danzmann, and R. Schnabel, Quantum-dense metrology, Nature Photon **7**, 626 (2013).
[5] S. L. Braunstein and H. Kimble, Dense coding for continuous variables, Phys. Rev. A **61**, 042302 (2000).
[6] S.-H. Tan, B. I. Erkmen, V. Giovannetti, S. Guha, S. Lloyd, L. Maccone, S. Pirandola, and J. H. Shapiro, Quantum Illumination with Gaussian States, Phys. Rev. Lett. **101**, 253601 (2008).
[7] C. W. Sandbo Chang, A. M. Vadiraj, J. Bourassa, B. Balaji, and C. M. Wilson, Quantum-enhanced noise radar, Appl. Phys. Lett. **114**, 112601 (2019).
[8] S. Barzanjeh, S. Pirandola, D. Vitali, and J. M. Fink, Microwave quantum illumination using a digital receiver, Sci. Adv. **6**, eabb0451 (2020).
[9] Z. Y. Ou, S. F. Pereira, H. J. Kimble, and K. C. Peng, Realization of the Einstein-Podolsky-Rosen Paradox for Continuous Variables, Phys. Rev. Lett. **68**, 3663 (1992).
[10] C. F. McCormick, V. Boyer, E. Arimondo, and P. D. Lett, Strong relative intensity squeezing by four-wave mixing in rubidium vapor, Opt. Lett. **32**, 178 (2007).
[11] C. Eichler, D. Bozyigit, C. Lang, M. Baur, L. Steffen, J. M. Fink, S. Filipp, and A. Wallraff, Observation of Two-Mode Squeezing in the Microwave Frequency Domain, Phys. Rev. Lett. **107**, 113601 (2011).
[12] M. Esposito, Arpit Ranadive, Luca Planat, Sébastien Leger, Dorian Fraudet, Vincent Jouanny, Olivier Buisson, Wiebke Guichard, Cécile Naud, José Aumentado, Florent Lecocq, and Nicolas Roch, Observation of Two-Mode Squeezing in a Traveling Wave Parametric Amplifier, Phys. Rev. Lett. **128**, 153603 (2022).
[13] A. Roy and M. Devoret, Introduction to parametric amplification of quantum signals with Josephson circuits, C. R. Physique **17**, 740 (2016).
[14] A. Blais, A. L. Grimsmo, S. M. Girvin, and A. Wallraff, Circuit quantum electrodynamics, Rev. Mod. Phys. **93**, 025005 (2021).
[15] B. A. Kochetov and A. Fedorov, Higher-order nonlinear effects in a Josephson parametric amplifier, Phys. Rev. B **92**, 224304 (2015).
[16] S. Boutin, D. M. Toyli, A. V. Venkatramani, A. W. Eddings, I. Siddiqi, and A. Blais, Effect of Higher-Order Nonlinearities on Amplification and Squeezing in Josephson Parametric Amplifiers, Phys. Rev. Appl. **8**, 054030 (2017).
[17] N. Bergeal, R. Vijay, V. E. Manucharyan, I. Siddiqi, R. J. Schoelkopf, S. M. Girvin, and M. H. Devoret, Analog information processing at the quantum limit with a Josephson ring modulator, Nature Phys. **6**, 296 (2010).
[18] N. Roch, E. Flurin, F. Nguyen, P. Morfin, P. Campagne-Ibarcq, M. H. Devoret, and B. Huard, Widely Tunable, Nondegenerate Three-Wave Mixing Microwave Device Operating near the Quantum Limit, Phys. Rev. Lett. **108**, 147701 (2012).
[19] C. Liu, T.-C. Chien, M. Hatridge, and D. Pekker, Optimizing Josephson-ring-modulator-based Josephson parametric amplifiers via full Hamiltonian control, Phys. Rev. A **101**, 042323 (2020).
[20] K. Mølmer, Y. Castin, and J. Dalibard, Monte Carlo wavefunction method in quantum optics, J. Opt. Soc. Am. B **10**, 524 (1993).
[21] Y. Castin and K. Mølmer, Monte Carlo Wave-Function Analysis of 3D Optical Molasses, Phys. Rev. Lett. **74**, 3772 (1995).
[22] A. Kamal, A. Marblestone, and M. Devoret, Signal-to-pump back action and self-oscillation in double-pump Josephson parametric amplifier, Phys. Rev. B **79**, 184301 (2009).
[23] K. E. Cahill and R. J. Glauber, Ordered expansions in boson amplitude operators, Phys. Rev. **177**, 1857 (1969).
[24] R. Simon, Peres-Horodecki Separability Criterion for Continuous Variable Systems, Phys. Rev. Lett. **84**, 2726 (2000).
[25] L.-M. Duan, G. Giedke, J. I. Cirac, and P. Zoller, Inseparability Criterion for Continuous Variable Systems, Phys. Rev. Lett. **84**, 2722 (2000).
[26] C. W. Gardiner and M. J. Collett, Input and output in damped quantum systems: Quantum stochastic differential equations and the master equation, Phys. Rev. A **31**, 3761 (1985).
[27] H. A. van der Vorst, Bi-CGSTAB: A fast and smoothly converging variant of Bi-CG for the solution of nonsymmetric linear systems, SIAM J. Sci. Stat. Comput. **13**, 631 (1992).
[28] Y. Saad, *Iterative Methods for Sparse Linear Systems* (Society for Industrial and Applied Mathematics, Philadelphia, 2003), 2nd ed.
[29] R. Schnabel, Squeezed states of light and their applications in laser interferometers, Phys. Rep. **684**, 1 (2017).
[30] C. M. Bender and S. Orszag, *Advanced Mathematical Methods for Scientists and Engineers: Asymptotic Methods and Perturbation Theory* (Springer, New York, 1999).